Augustana College
Augustana Digital Commons

Celebration of Learning

Optimizing UAV surveys for coastal morphodynamics: estimation of spatial uncertainty as a function of flight acquisition and post-processing factors

Mark Lundine
Augustana College, Rock Island Illinois

Follow this and additional works at: https://digitalcommons.augustana.edu/celebrationoflearning
Part of the Geomorphology Commons

Optimizing UAV surveys for coastal morphodynamics: estimation of spatial uncertainty as a function of flight acquisition and post processing factors

a senior thesis written by

Mark Lundine

in partial fulfillment of the graduation requirements
for the major in geology

Augustana College
Rock Island, IL 61201

2018

Abstract

Recent developments in unmanned aerial vehicles (UAVs) and photogrammetry software enable the rapid collection of aerial photography and video over study areas of varying sizes, thereby providing ease of use and accessibility to coastal research groups. However, there remains uncertainty over UAV survey techniques, with disagreement on specific flight patterns, flight altitudes, photograph amounts, ground control point (GCP) amounts, GCP spacing schemes, drone models, and which SfM software to use, amongst other study-specific parameters.

To address the methodological differences amongst research groups, this study uses varying collection parameters to investigate the error of drone-derived spatial data. A controlled field test (of 1.2 hectares) was performed to determine SfM's sensitivity to the following flight parameters: flight altitude (60-m, 80-m, 120-m), photo overlap (70%, 75%, 80%), drone model (DJI Phantom quadcopter, Sensefly eBee RTK fixed-wing), SfM software (PhotoScan, Pix4D), number of GCPs (4-34), and spacing scheme of GCPs (even, random). Through comparisons of the root mean squared error (RMSE) relative to the GCPs, flight altitude affected error significantly (>1-cm RMSE difference between 60-m and 120-m) while photo overlap was the least significant parameter (only 4-mm RMSE difference between 70% and 80% overlap). Different drone models, and thereby different cameras, along with varying photogrammetry software, affected RMSE significantly (>3-cm RMSE differences). Surprisingly, GCP spacing schemes were insignificant to error sensitivity (<1 mm RMSE differences). Final analysis determined six GCPs per hectare of land surveyed to be the most efficient, while flight altitudes of 80 meters with 70% overlap were the most

efficient for flight time (~4 min), ground resolution (3.42-cm/pixel), and RMSE (4-cm). This study can be immediately referenced in future studies for its insight on conducting efficient and low-error UAV surveys.

1. Introduction

1.1 UAV/SfM Background

Throughout the past several years, an exciting and technologically savvy paradigm shift in the geosciences has been occurring. This shift refers to the drastic increase in the use of unmanned aerial vehicles (UAVs) along with structure from motion (SfM) to study various geoscientific problems. UAVs and SfM have become more readily available to scientists less experienced with aviation and computer vision techniques, with advancements in automatic flight-planning as well as data-processing software. These technological advancements have created great potential for the use of UAVs and SfM in the geosciences.

Like many scientific instruments, UAVs were developed by the military for use in unmanned reconnaissance in combat areas (Nex and Remondino 2013). UAVs have now transformed into a tool for geoscientists, allowing for rapid photography and video capture in various environments. When these photographs are processed through SfM software, they can be used to create a variety of digital outputs that provide topographic and ecological information. These products can then be analyzed to map and denote precise changes in surface areas, volumes, slopes, and vegetation amounts, among many other geoscientific applications.

While photogrammetric methods have existed in the geosciences for decades, the digital construction of 3D point clouds, 3D meshes, digital elevation models, and orthomosaics from UAV-captured photosets is a recent phenomenon. A search of "drone OR UAV" in ProQuest's geoscience database GeoRef resulted in 145 publications, with 130 of them coming after January of 2011. As for SfM, a search in the same database gave similar results, with 151 of 191 publications being written from 2011 and on. In academic geosciences, drones are new and highly-desired tools, which can be easily integrated with structure from motion algorithms to produce a variety of useful, digitized, three-dimensional spatial data.

Some publications using drones and/or SfM include studies on beach morphology and coastal storm-response (Dohner *et al.* 2016, Casella *et al.* 2016, Scarelli *et al.* 2017, Turner *et al.* 2016), a study on the topography of open-pit mines (Esposito *et al.* 2017), paleontological studies on modelling dinosaur footprints and bones (Citton *et al.* 2015; Hyatt 2017), 3D reconstruction of seafloors for mapping shipwrecks (Issaris 2015), extraction of bathymetric data on shallow streams and the nearshore, (Dietrich 2016, Holman *et al.* 2013, Holman *et al.* 2017), as well as for the monitoring of the rapidly changing topography of volcanoes (Gomez 2012, Derrien *et al.* 2015). Each study referenced above reiterated the cost-effectiveness as well as the quickness in data processing involved with SfM when compared to terrestrial or aerial LiDAR surveys.

The data produced through UAV surveys and SfM is similar to the results of laser scanning methods, like terrestrial and aerial LiDAR (Long *et al.* 2016, Westoby *et al.* 2012). Instead of using the reflectance properties of a laser to scan an area, SfM uses information extracted from overlapping 2D images to construct 3D structure. Most SfM software use a

feature extraction algorithm, where overlapping photos are scanned for common "features", which often include elements in the photos with sharp edges, distinct colors, or drastic slope changes. These features are easily recognized and therefore their higher prevalence in a photoset will result in more accurate three-dimensional reconstructions (Carrivick *et al.* 2012). Photosets lacking textured features and experiencing illumination changes, as well as being taken under varied camera geometries will result in inadequate 3D reconstructions (Harwin and Lucieer 2012). While converging, off-nadir camera angles result in the most accurate 3D models, parallel and nadir angles can produce models that are almost as accurate (James and Robson 2014). For a UAV survey, the most practical camera geometry is one using parallel and nadir angles. For the 3D outputs to be correctly georeferenced and for the data to be placed into a non-arbitrary coordinate system, either the 3D position of the cameras need to be known or the 3D position of ground control points (GCPs), targets placed in the study area that can be seen in multiple photos in the overall photoset, must be established.

The typical reconstruction algorithm is as follows (see Figure 1): input of photoset; initial feature detection; matching of features in overlapping photos; filtering out poor or distorted matches; construction of 3D geometry, camera positions, and internal camera parameters; input of GCPs; scaling and georeferencing of the 3D point cloud; and then the final output is a georeferenced point cloud (Carrivick *et al.* 2012).

The SfM method is more cost-effective and more feasible in rugged environments when compared to laser scanning. Aerial LiDAR surveys require substantial funds as well as a trained pilot, while terrestrial LiDAR surveys are costly and involve the transfer of heavy and fragile pieces of equipment (Carrivick *et al.* 2012). Both of these laser scanning

approaches require meticulous planning and several scientists to ensure a successful survey. This makes the laser scanning approach incredibly difficult to accomplish rapid data acquisition in rough terrain or in rapidly changing environments.
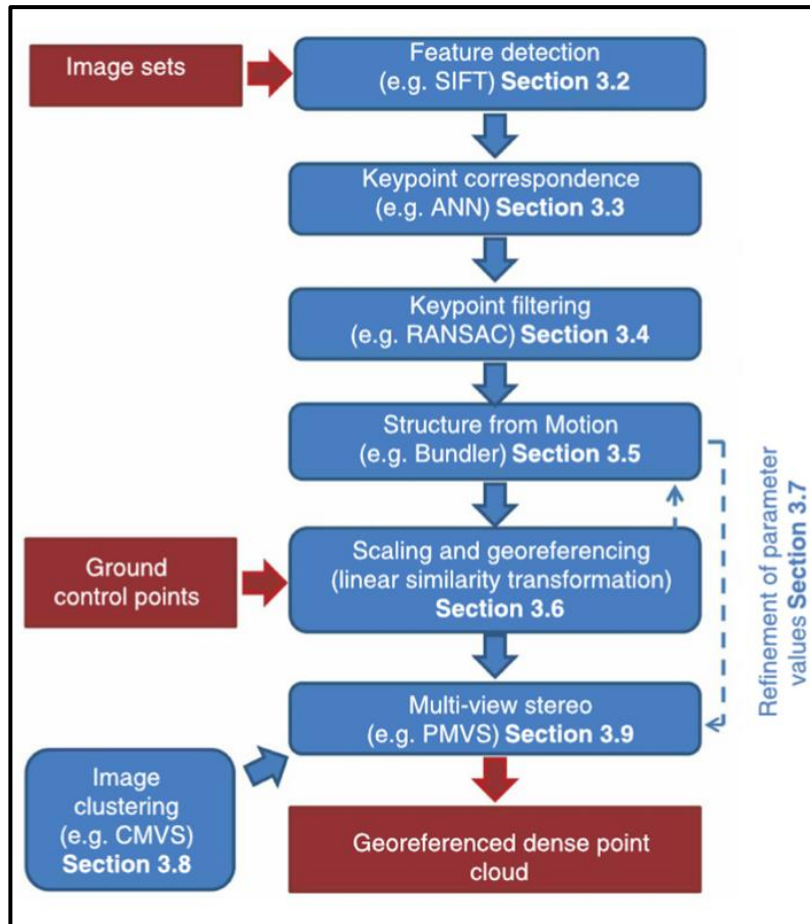

Figure 1: Typical SfM algorithm (Carrivick *et al.* 2012).

1.2 Past Studies on UAV/SfM Accuracy

Previous studies were conducted on UAV/SfM model accuracy, with many of them being small portions of studies done on various geoscientific problems. Most geoscientific studies that have used the UAV/SfM methodology have included error metrics for their 3D models, but different studies have used different UAV types, different processing software,

different GCP placing schemes, different GCP amounts, different UAV altitudes, and different photograph overlap amounts. Consequently, a single paper cannot provide sufficient information on the optimum UAV survey, due to the variation in the variables listed above, as well as the different environments these studies take place in. In addition, the comparison data collection methods (LiDAR, RTK GPS, Total Station, etc.) and the error metrics provided (RMSE, absolute error, mean error, etc.) vary from study to study. For a summary of past studies on UAV/SfM model accuracy, see Appendix A.

As an example of the predicament, a 2013 study on a ~2-km^2 dunefield, using 28 GCPs and a UAV altitude of 200-m, managed to produce an elevation root mean square error of 0.29-m (Hugenholtz *et al.* 2013). A paper from 2016 studying beach morphology, using no GCPs and a UAV altitude of 100-m, produced a mean elevation error of 0.026-m (Turner *et. al* 2016). This 2016 paper did not use any GCPs because their UAV was equipped with an RTK GPS unit, which provided them with high accuracy coordinates of their camera positions. It should also be noted that these two studies used different processing software; the former used Trimble Impho, while the latter used Pix4D. The 2016 study fails to provide an accurate error metric; the mean elevation error takes positive and negative values, which will result in a mean error closer to zero. This is misleading, as the models could have absolute errors far from zero.

Both studies only provide elevation error metrics, which eliminates vital information on the horizontal accuracy of their models. Studies that provide error metrics only include elevation errors, and the parameters for each study are different, which leads to little consensus on the optimum parameters to minimize model error. Figuring out the optimum parameters, thus far, has involved comparing literature results, peer to peer discussion, and

experimentation with different altitudes, overlap amounts, GCP spacing schemes, and GCP amounts. There has been a limited amount of papers done specifically to quantify the error of UAV/SfM models as well as to investigate the optimum altitude, overlap amount, number of GCPs, and the best GCP spacing schemes for an accurate survey.

In a 2016 study, the effect of GCP amount and placement was investigated (Tonkin and Midgley 2016). This study was able to show a clear decrease in elevation error with respect to increasing GCP amounts, but with a less substantial decrease as GCP amounts reached an "excessive" level. They were also able to determine that the best GCP spacing scheme was one that provided "uniform" coverage throughout the study area. Another paper, from 2016, was able to show differences in model errors between two processing software suites (Agisoft and MicMac) (Jaud *et al.* 2016). Agisoft was shown to produce models with slightly higher horizontal and elevation RMSEs (0.045-m, 0.039-m) when compared to MicMac (0.035-m, 0.032-m). It should be noted that their comparison data consisted of dGPS coordinates. When their models were compared to TLS data, however, the Agisoft models were closer in mean difference to the TLS models (0.05-m) when compared to the MicMac models (0.22-m). This study shows that different processing software can produce different amounts of model error, but it also shows that different comparison data collection methods will result in different error amounts.

While all of these studies provide vital information on optimizing the parameters involved in a UAV survey, the amount of data provided from these studies is limited, and several questions are still left unanswered: what is the optimum UAV altitude; how much overlap is needed in the photography; are the differences in error produced by different software statistically significant; how many GCPs are needed per unit of area; and should the

GCPs be spaced in equal increments uniformly throughout the study area, or can they be placed in random locations? The purpose of this study is to investigate the effects of these parameters on model accuracy, to provide various error metrics on x, y, and z coordinates, to make additional contributions to the data on UAV/SfM models, and to provide substantial insight into how to optimize survey parameters and minimize the error in 3D reconstructions.

2. Study Area

Data collection was conducted in a grass field outside of the Otis H. Smith Laboratory, located at the Hugh R. Sharp campus, which houses the University of Delaware College of Earth, Ocean, and Environment, and is less than a kilometer southwest of Delaware Bay (see Figure 2). The field is approximately 100-m by 120-m (0.012-km^2), with little topographic variability, ranging from 2.912-m to 4.20-m in elevation, and with almost no trees or man-made structures casting shadows anywhere in its vicinity. The lack of shadows throughout the field made it advantageous for capturing useful photosets to be converted into 3D outputs (point clouds, meshes, DEMs, etc.). The field's nearly constant elevation, its lack of highly detailed vegetation (like trees and bushes), along with the absence of shadow-casting structures within the field made it an ideal area to conduct multiple drone surveys for a detailed error analysis.
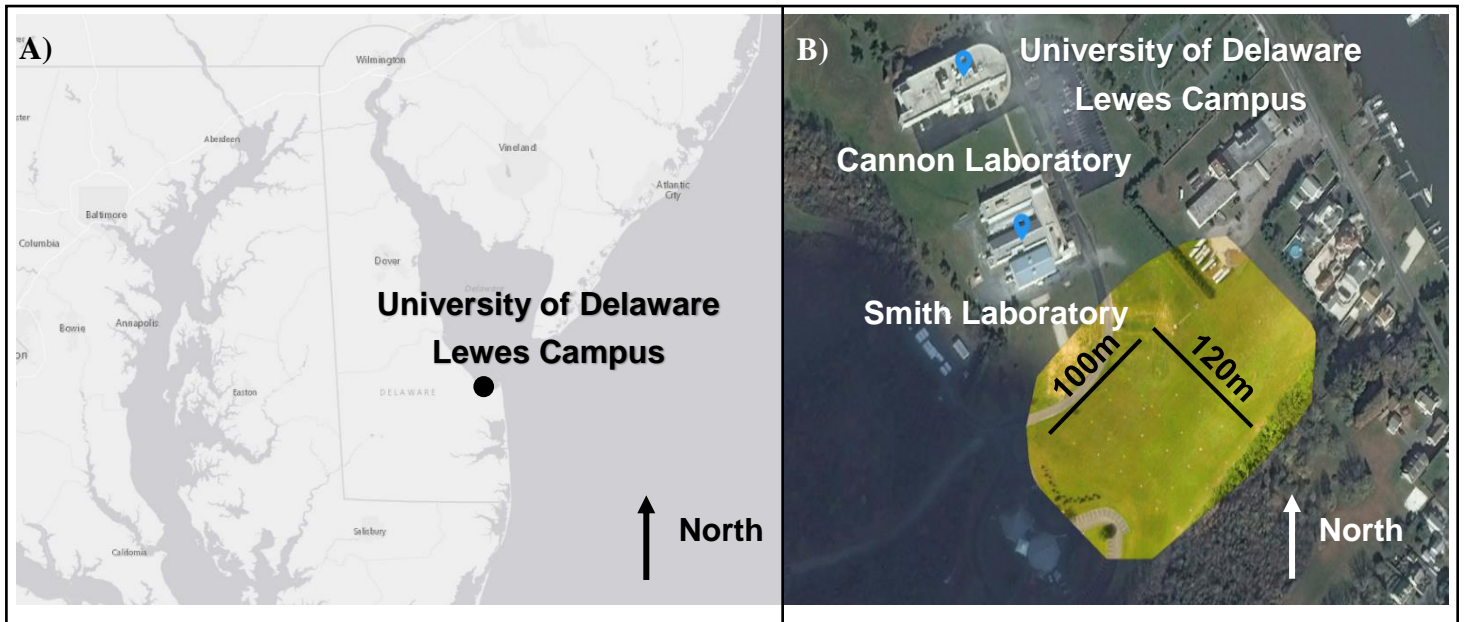
Figure 2: Study area. A) University of Delaware at southwest corner of Delaware Bay. B) Orthomosaic of study area.

3. Methodology

3.1 Ground control point placement

Within the 100m by 120m rectangular field established for the drone surveys, 35[*] GCPs were placed to georeference and scale the models. The GCPs were made either from black and white tarps placed upon the field or from eco-friendly paint applied directly to the field. Each GCP was approximately one meter in length and width. See Figure 3 for examples of different GCPs. First, 30 GCPs were placed evenly throughout the field, making

Figure 3: Examples of GCPs.

*One GCP was not used due to corrupted data.

six rows of five GCPs, and then five more were added in a cluster between the second and

third rows. The additional five GCPs were placed to experiment with different paint colors,

in order to determine the most easily visible paint from the aerial photography. The first

thirty GCPs were assigned numerical names (1-30), while the last five were assigned color

names and a Roman numeral name (Blue, Red, Orange, Yellow, I). Giving these GCPs

names aided in identifying them in the aerial photography, as their names were visible in the

photographs. See Figure 4 for the layout of the GCPs throughout the study area.
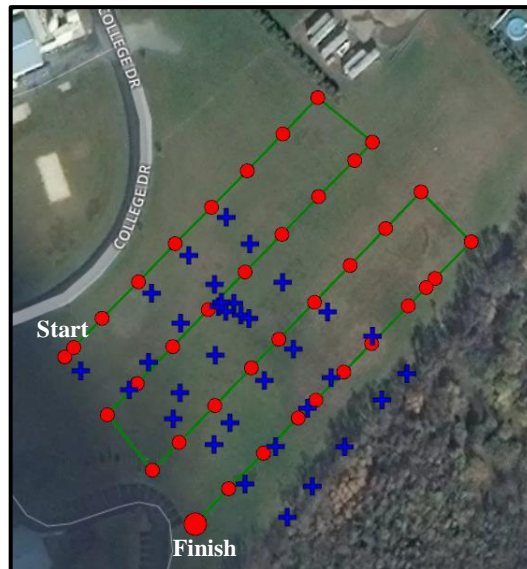

Figure 4: Example flight plan and placement of GCPs; green line indicates flight path; red circles indicate photograph positions; blue crosses indicate GCP locations.

Once the GCPs were laid out, their World Geodetic System 1984 (WGS 84)

geographic coordinates (latitude, longitude, elevation) were recorded using a Topcon GR 5

Real Time Kinematic (RTK) GPS unit with its receiver extended on a 2-m pole. The Topcon

GR 5 has a horizontal accuracy of 0.005-m and a vertical accuracy of 0.01-m. These

geographic coordinates were then converted into Universal Transverse Mercator (UTM)

coordinates to facilitate their use in 2D and 3D model projection as well as in error

measurement. The UTM coordinates were then arranged into a spreadsheet by their GCP

name, easting coordinate (X), northing coordinate (Y), and elevation (Z).   Arranging the

coordinates in this fashion allows for the rapid implementation of GCPs into SfM software.

3.2 UAV surveys

A total of six UAV surveys were done on the study area, five of which used a DJI

Phantom 3 Advanced quadcopter, while the sixth used a senseFly eBee RTK fixed-wing

drone. The Phantom is equipped with a 12.4-megapixel RGB camera, mounted on a 3-axis

gimbal on the drone's underside, allowing for tilted, oblique, and nadir aerial photography.

When the Phantom captures photographs, it maintains a constant position during each

photograph before moving to the next photograph location. This eliminates blurred images,

which can create difficulty in 3D reconstruction. The eBee is equipped with a 20-megapixel

RGB camera, mounted within the drone's body, with the lens facing downward out of its

underside. When the eBee captures photographs, it pitches up to gather near-nadir

photography; this can create somewhat blurred images, as the drone is in motion as it

captures each image.

Each flight was programmed using the automatic flight planning app *Maps Made

Easy*, which allows its users to specify flight areas, flight speeds, flight altitudes, and amount

of overlap in the aerial photography. Each flight plan used the "lawn-mowing" flight pattern,

where the drone surveyed the field in a series of antiparallel straight lines (see Figure 4).

Their flight parameters (UAV type, altitude, along-track overlap, across-track overlap,

number of photographs, flight time) are described in Table 1. The five quadcopter surveys

were conducted on June 7th, 2017, during the early afternoon, while the eBee survey was done on June 8th, 2017, during the mid-afternoon. All six surveys were conducted under some cloud cover but with ideal wind conditions, allowing for controlled flights as well as clear photography. To maintain consistent exposure settings on the two drones' cameras, the automatic setting was switched to "cloudy". This was done to avoid any mid-survey differences in photography color due to the camera automatically adjusting the exposure settings under different lighting. The six surveys served to investigate the differences between different altitudes, different overlap amounts, and different drone types in terms of model accuracy.

Table 1: UAV flight specifications.

UAV Type	Altitude (m)	Along-Track Overlap (%)	Across-Track Overlap (%)	Number of Photos	Flight Time (min)	Ground Sampling Distance (cm/pixel)
Quadcopter	60	70	75	42	5.4	2.51
Quadcopter	80	70	75	23	4.5	3.30
Quadcopter	80	75	80	27	4.8	3.24
Quadcopter	80	80	80	38	4.8	3.30
Quadcopter	120	70	75	11	5	4.70
Fixed-wing	80	70	75	38	4	2.19

3.3 Image processing

This project aimed to investigate the effects of altitude, photography overlap, number of GCPs, spacing of GCPs, drone type, and GCP type on model accuracy. First, each photoset was initially processed in the Pix4D Cloud software without any GCPs to find the best 3D reconstruction based only on the photo quality and the internal GPS systems on the quadcopter and the fixed-wing drone. This software allows its users to input photography to a cloud service that processes the data online, producing orthomosaics, digital terrain maps, and 3D models without requiring any computing costs or management by its users. It is useful for rapid initial data processing. After the initial Pix4DCloud processing, the quadcopter survey done at 80-m altitude with 80% across-track overlap and 80% along-track overlap was determined to be the most accurate survey, and thus was used to analyze the effects of GCP amount and spacing. This flight, after initial processing, produced the highest number of 2D and 3D keypoints (matches) relative to the other flights, which made it, initially, the most accurate reconstruction of the field.

To investigate the effects of GCP amounts and spacing, the survey done at 80-m altitude with 80% across-track overlap and 80% along-track overlap was processed in Pix4D using various amounts of GCPs. For each GCP amount, the dataset was processed with evenly spaced GCPs throughout the field, and then the dataset was processed with randomly spaced GCPs throughout the field. The random GCPs were selected using a Java program that accepts a number of GCPs, and then returns which GCPs (1-34) to include in processing

(using the Java pseudo-random number generator). See Figure 5 for an example of an even vs. random GCP spacing scheme.
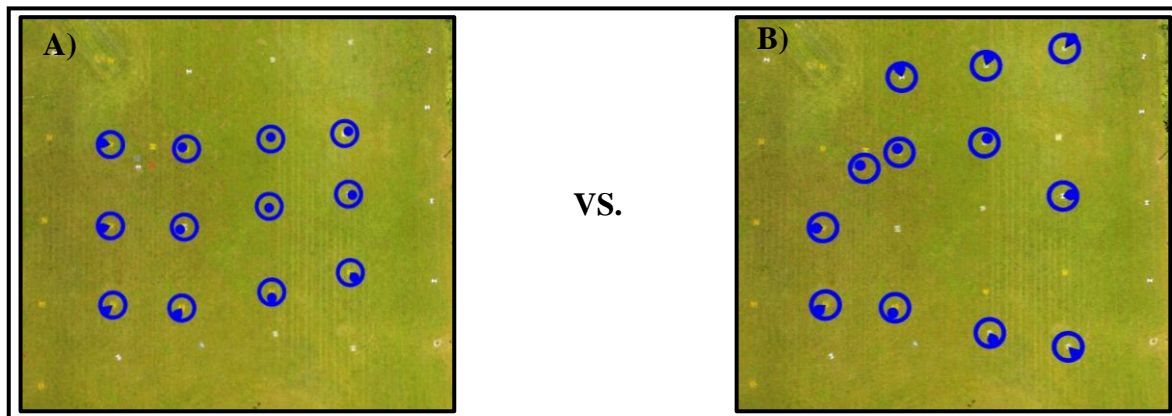

Figure 5: A) Evenly spaced GCPs. B) Randomly spaced GCPs.

Second, the three separate quadcopter surveys done at different altitudes (all at 80% across-track overlap and 80% along-track overlap) were processed with the maximum number of GCPs (34) to investigate the effect of altitude on model accuracy.

Third, the three separate quadcopter surveys done with different overlap amounts (all at 80-m altitude) were processed with the maximum number of GCPs (34) to investigate the effect of photography overlap on model error.

Fourth, the fixed-wing survey was processed with no GCPs to compare this drone's RTK GPS data with the ground collected RTK GPS data, as well as to assess the differences in model accuracy between the fixed-wing drone and the quadcopter.

Last, the 80-m altitude, 70% across-track, and 75% overlap survey was processed with 34 GCPs in Agisoft PhotoScan to show variations in model accuracy between different processing software. Agisoft PhotoScan is processed by the user in a similar manner as in Pix4D, allowing its users to import and identify the GCP locations within the models.

3.4 Measuring model error

Error in each processed dataset was calculated by comparing each GCP's RTK recorded XYZ coordinates with the XYZ coordinates computed through the Pix4D and Agisoft PhotoScan SfM software. For each GCP integrated into the processed data, the error was automatically calculated by the software. For GCPs not integrated into the processed data, the error was calculated by identifying the GCP within the model, selecting the point representing that GCP's location, and then finding the difference between that point's RTK GPS position and its computed position. The following metrics were calculated to quantify the error involved with each RTK point (n = 34) within each 3D reconstruction:

- X, Y, Z error ($\varepsilon_{X,Y,Z}$): (1)

$$\varepsilon_X = X_{RTK} - X_{Computed}$$

$$\varepsilon_Y = Y_{RTK} - Y_{Computed}$$

$$\varepsilon_Z = Z_{RTK} - Z_{Computed}$$

- X, Y, Z absolute error ($\alpha_{X,Y,Z}$): (2)

$$\alpha_X = \left| X_{RTK} - X_{Computed} \right|$$

$$\alpha_Y = \left| Y_{RTK} - Y_{Computed} \right|$$

$$\alpha_Z = \left| Z_{RTK} - Z_{Computed} \right|$$

The following metrics were calculated to quantify the average errors for each 3D construction:

- X, Y, Z root mean squared error ($RMSE_{X,Y,Z}$):

    (3)

$$RMSE_X = \sqrt{\frac{\sum_{i=1}^{n}(X_{RTK_i} - X_{Computed_i})^2}{n}}$$

$$RMSE_Y = \sqrt{\frac{\sum_{i=1}^{n}(Y_{RTK_i} - Y_{Computed_i})^2}{n}}$$

$$RMSE_Z = \sqrt{\frac{\sum_{i=1}^{n}(Z_{RTK_i} - Z_{Computed_i})^2}{n}}$$

- Mean RMSE: (4)

$$Mean\ RMSE = \frac{RMSE_X + RMSE_Y + RMSE_Z}{3}$$

- X, Y, Z mean absolute error ($MAE_{X,Y,Z}$): (5)

$$MAE_X = \frac{\sum_{i=1}^{n}\left|X_{RTK_i} - X_{Computed_i}\right|}{n}$$

$$MAE_Y = \frac{\sum_{i=1}^{n}\left|Y_{RTK_i} - Y_{Computed_i}\right|}{n}$$

$$MAE_Z = \frac{\sum_{i=1}^{n}\left|Z_{RTK_i} - Z_{Computed_i}\right|}{n}$$

- Mean MAE (*Mean MAE*): (6)

$$Mean\ MAE = \frac{MAE_X + MAE_Y + MAE_Z}{3}$$

3.5 Statistical analyses

Several single factor and two-factor univariate analysis of variance tests (ANOVA) were performed on the datasets, using Excel 2016. The first analyses were done on the 80-m, 80% across-track and 80% along-track overlap datasets, where GCP amount and spacing was varied. The analyses used were two-factor ANOVAs with replication. For the first

16

ANOVA, the first factor was GCP spacing (even or random), while the second factor was GCP amount. The dependent variable was the X-absolute error (α_X) for each point. For the second and third ANOVAs, the factors were the same as above, with the second dependent variable being the Y-absolute error (α_Y), and the third dependent variable being the Z-absolute error (α_Z).

To investigate the effects of adding more than six GCPs, the same two-factor ANOVAs were performed as above, except without the zero GCP data and the four GCP data. This was done to determine at what point adding more GCPs becomes excessive.

The next statistical analysis was done on the flights where overlap was kept constant (70% along-track, 75% across-track), but the altitude was varied (60-m, 80-m, 120-m). The test was a single-factor ANOVA, where the factor was altitude and the dependent variable was absolute error. In this test, α_X, α_Y, α_Z, were grouped together, giving a sample size of n = 102 for each of the three separate altitude datasets.

The next statistical analysis was done on the flights where altitude was kept constant (80-m), but overlap was varied. The test was a single-factor ANOVA, where the factor was overlap and the dependent variable was X, Y, and Z absolute error, in the same way as the ANOVA done on the different altitude datasets.

The final two statistical tests performed were both single-factor ANOVAs, where one test was done to compare the absolute error of the eBee flight with the absolute error of a Phantom flight (both flights were at 80-m, 70% along-track overlap, and 75% across-track

Table 2: Statistical tests performed.

Test	Factor(s) with levels	Dependent variable (s)
One-way ANOVA	Altitude: 60-m, 80-m, 120-m	X, Y, Z absolute error
One-way ANOVA	Overlap % (Along/Across): 70/75, 75/80, 80/80	X, Y, Z absolute error
Two-way ANOVA with replication (3 tests done for X, Y, and Z)	# of GCPs: 0, 4, 6, 8, 10, 12, 14, 20, 24, 30, 34 Spacing: even, random	X absolute error Y absolute error Z absolute error
Two-way ANOVA with replication (3 tests done for X, Y, and Z)	# of GCPs: 6, 8, 10, 12, 14, 20, 24, 30, 34 Spacing: even, random	X absolute error Y absolute error Z absolute error
One-way ANOVA	Drone type: quadcopter, fixed wing	X, Y, Z absolute error
One-way ANOVA	Software: Pix4D Desktop, Agisoft PhotoScan	X, Y, Z absolute error

overlap). The other test was done to compare the absolute error computed through different processing software (Pix4D and Agisoft).

See Table 2 for a description of the various ANOVAs performed in this study.

3.6 Raster and Point Cloud Comparisons

Raster and point cloud comparisons were made between the following datasets:

1.   Quadcopter vs. fixed-wing

2.   Pix4D Desktop vs. Agisoft PhotoScan

3.   6 GCPs vs 0 GCPs

4.   6 GCPs vs. 4 GCPs

5.   60-m flight vs. 80-m flight

6.   60-m flight vs. 120-m flight

Elevation rasters for each processed dataset were constructed in ArcMap to compute elevation differences between different datasets. Each raster constructed had a grid-spacing of 0.05-m by 0.05-m and used the "Natural Neighbor" interpolation method. Elevation differences were computed using the Minus function, found in the Raster Math toolbox.

Point cloud comparisons were made in the free and open-source software CloudCompare, using the cloud to cloud distance tool. This tool provides X, Y, and Z distances between all of the points of two different point clouds, which allowed us to determine horizontal and elevation differences between various pairs of point clouds processed for this study, as well as the locations of these differences within the models.

4. Results

4.1 Altitude

The average model error increased with respect to increasing altitude (see Figure 6), with the most drastic error increases coming from the z-coordinates. From the single-factor ANOVA results, changing the UAV altitude did result in statistically significant differences in absolute error (p-value = 0.011, see Table 3).
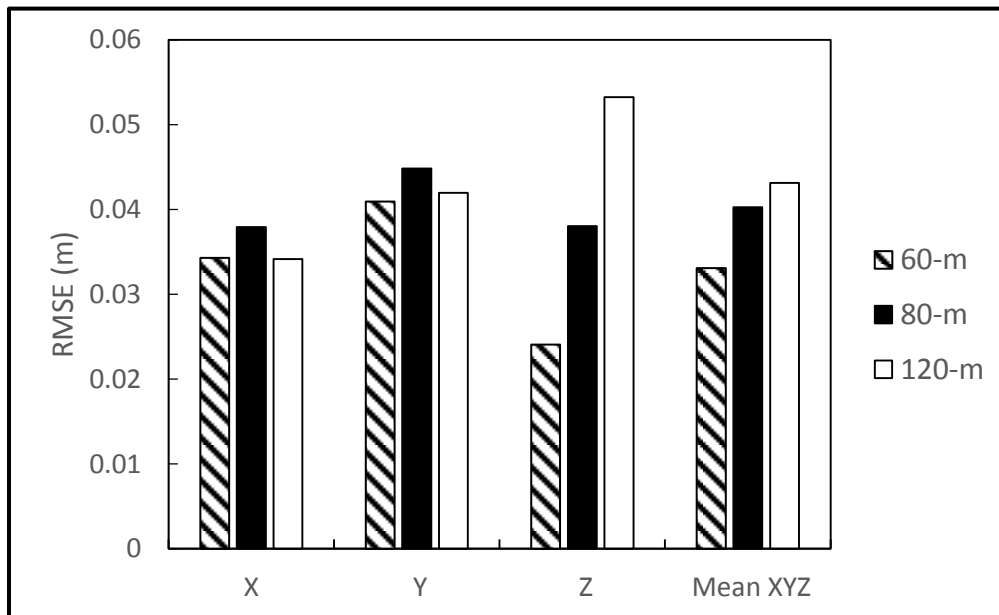

Figure 6: Altitude and RMSE.

Test	Dependent variable	Factor(s) with levels	P-value	% of Variance	Significance
One-way ANOVA	X, Y, Z absolute error	Altitude: 60-m, 80-m, 120-m	0.011	2.96	Significantly different
One-way ANOVA	X, Y, Z absolute error	Overlap: 70/75, 75/80, 80/80	0.56	0.39	Not significantly different
Two-way ANOVA with replication	X absolute error	# of GCPs: 0, 4, 6, 8, 10, 12, 14, 20, 24, 30, 34	3.10×10^{-143}	61.51	Significantly different
		Spacing: even, random	0.97	6.07×10^{-5}	Not significantly different
Two-way ANOVA with replication	Y absolute error	# of GCPs: 0, 4, 6, 8, 10, 12, 14, 20, 24, 30, 34	2.30×10^{-147}	62.50	Significantly different
		Spacing: even, random	0.97	0.00018	Not significantly different
Two-way ANOVA with replication	Z absolute error	# of GCPs: 0, 4, 6, 8, 10, 12, 14, 20, 24, 30, 34	0.00	99.98	Significantly different
		Spacing: even, random	0.71	2.29×10^{-5}	Not significantly different
Two-way ANOVA with replication	X absolute error	# of GCPs: 6, 8, 10, 12, 14, 20, 24, 30, 34	0.36	1.49	Not significantly different
		Spacing: even, random	0.99	5.90×10^{-5}	Not significantly different
Two-way ANOVA with replication	Y absolute error	# of GCPs: 6, 8, 10, 12, 14, 20, 24, 30, 34	0.90	0.58	Not significantly different
		Spacing: even, random	0.64	0.038	Not significantly different
Two-way ANOVA with replication	Z absolute error	# of GCPs: 6, 8, 10, 12, 14, 20, 24, 30, 34	0.15	1.97	Not significantly different
		Spacing: even, random	0.074	0.52	Not significantly different
One-way ANOVA	X, Y, Z absolute error	Drone type: quadcopter, fixed-wing	1.72×10^{-13}	29.79	Significantly different
One-way ANOVA	X, Y, Z absolute error	Software: Pix4D Desktop, Agisoft PhotoScan	0.00070	5.54	Significantly different

4.2 Overlap

The average model error decreased with respect to increasing photography overlap amounts (see Figure 7), with the errors decreasing at similar increments for all three coordinate directions. From the single factor ANOVA results, the different photography overlap amounts did not produce absolute errors with statistically significant differences (p-value = 0.56, see Table 3).
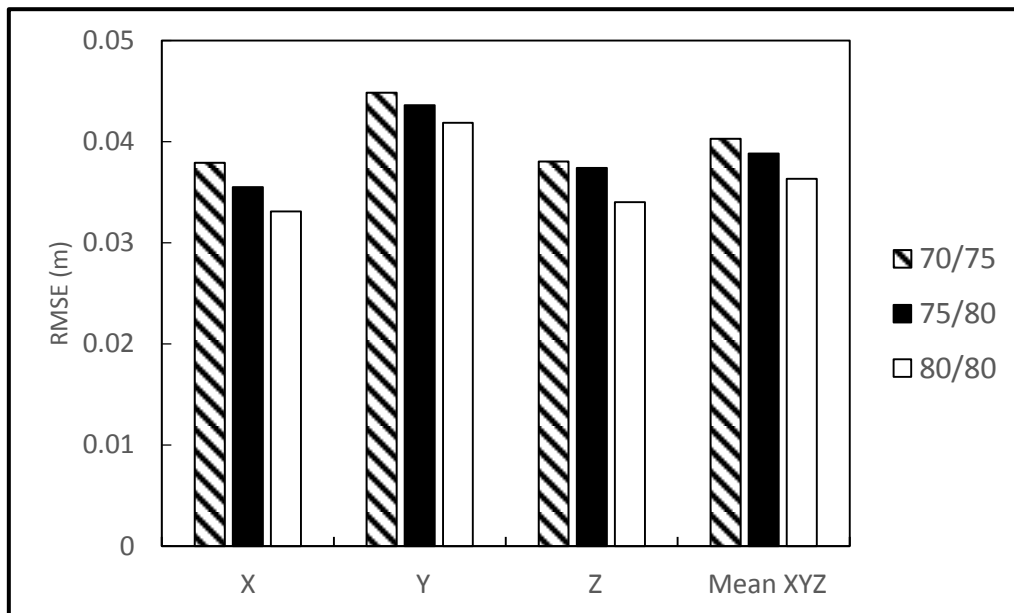

Figure 7: Photography overlap percentage and RMSE. Note the small decreases in RMSE with increasing overlap percentages.

4.3 GCP Amount and Spacing

With zero GCPs, the mean RMSE was 3.778-m, which then decreased to 0.129-m with four GCPs, and then to 0.047-m with six GCPs (see Figure 8). When the dataset was processed with more than six GCPs, the decrease in error was slight and in some cases, error increased with additional GCPs. There was little difference in error between evenly spaced and randomly spaced GCPs; both spacing schemes experienced similar RMSE changes with increasing GCP amounts. (see Figure 9). At lower GCP amounts, most of the error is coming from the z-coordinates (see Figures 10 and 11), while at the highest GCP amounts, the Z-coordinates are producing the least amount of error, with more error coming from the X- and Y-coordinates. From the two-factor ANOVA results, for the X-coordinates, the difference in absolute error between even-spacing schemes and random-spacing schemes was not statistically significant (p-value = 0.97), while the difference in error between different GCP amounts was statistically significant (p-value $= 3.10 \times 10^{-143}$). For the Y- and Z-coordinates, the statistical results were the same: a statistically significant difference for different GCP amounts but not a statically significant difference for the two GCP spacing schemes (see Table 3).

When the zero and four GCP datasets were not included in the two-factor ANOVA, the difference in absolute error between even and random spacing schemes was again, not statistically significant for X, Y, and Z coordinates. However, the difference in X, Y, and Z absolute errors between different GCP amounts was also not statistically significant (see Table 3).
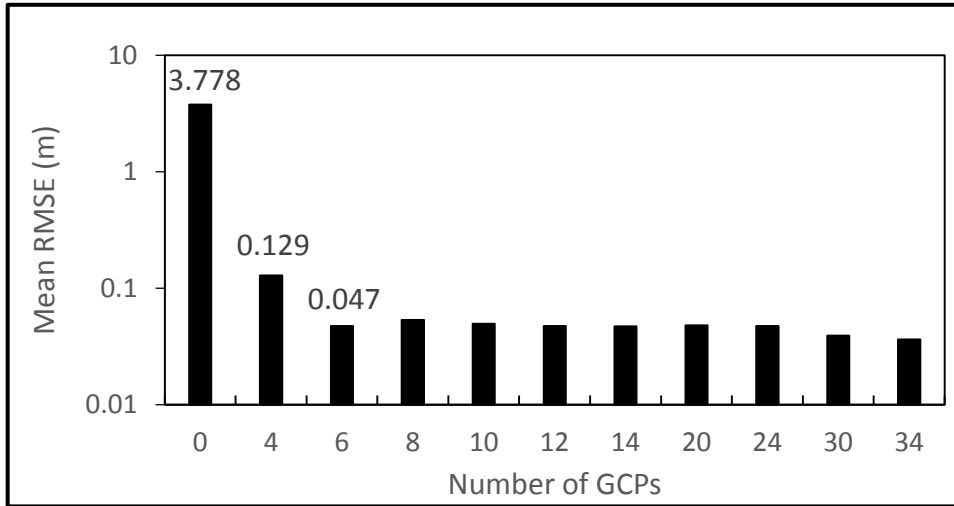
Figure 8: Evenly spaced GCP amount and mean RMSE. Y-axis has a base-10 logarithmic scale. Note great RMSE change from 0 to 4 to 6 GCPs, but little change after 6 GCPs.
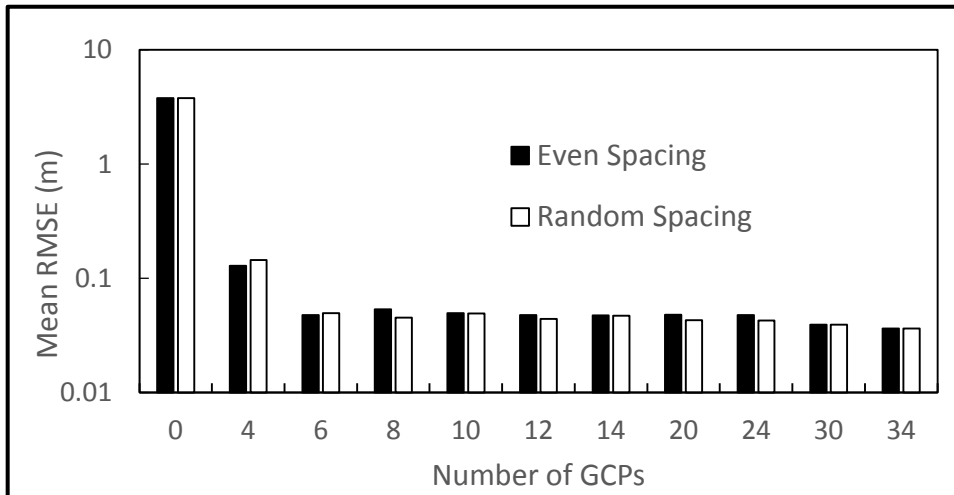

Figure 9: GCP spacing and mean RMSE. Y-axis has a base-10 logarithmic scale. Note similarity between even and random spacing RMSE.
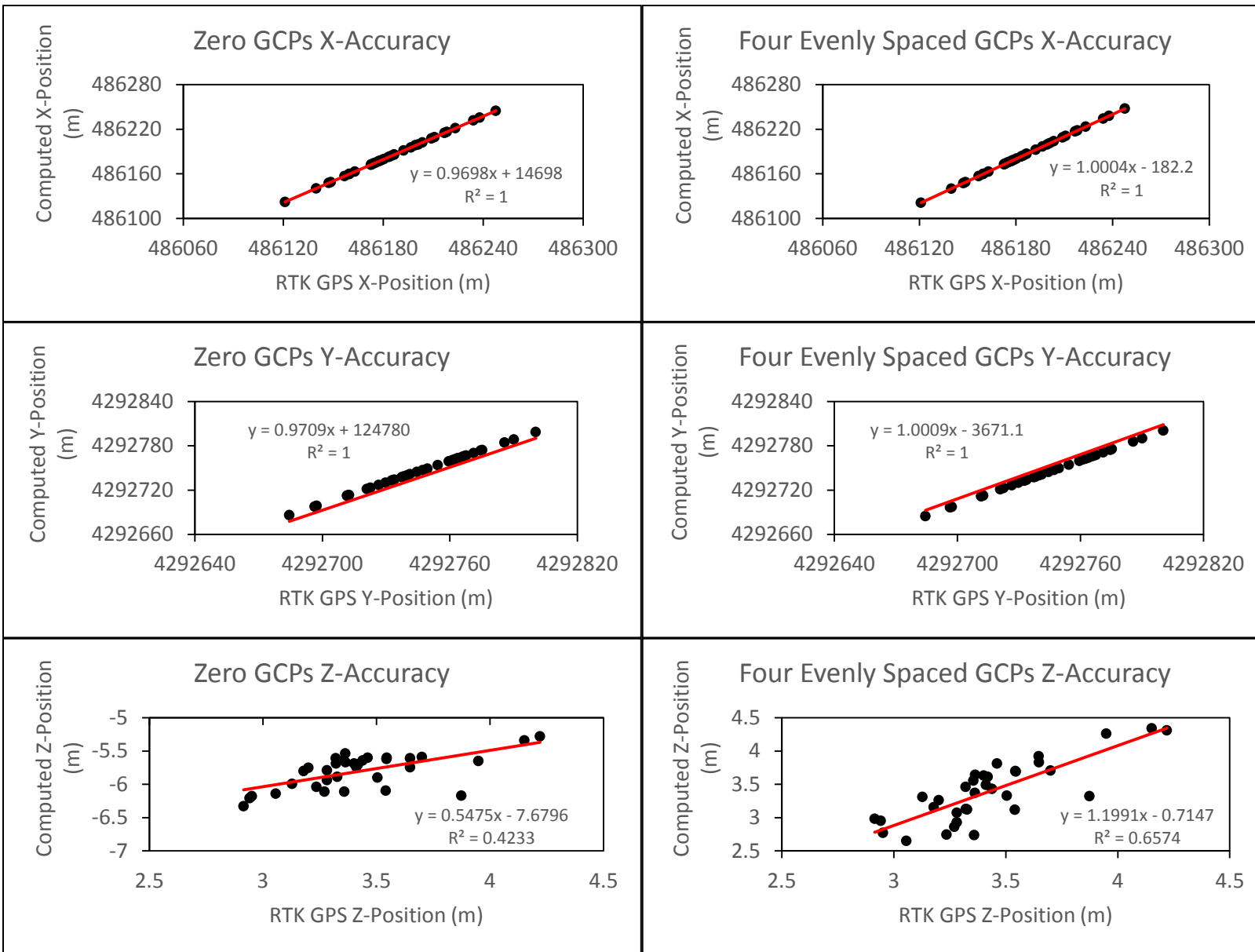
Figure 10: Changes in XYZ model accuracy with different GCP amounts. The greatest improvements in model accuracy were observed in the Z-coordinates with increasing GCP amounts. At four GCPs, there is low variability between the RTK and computed X & Y positions, but there is still high variability in the Z-coordinates.
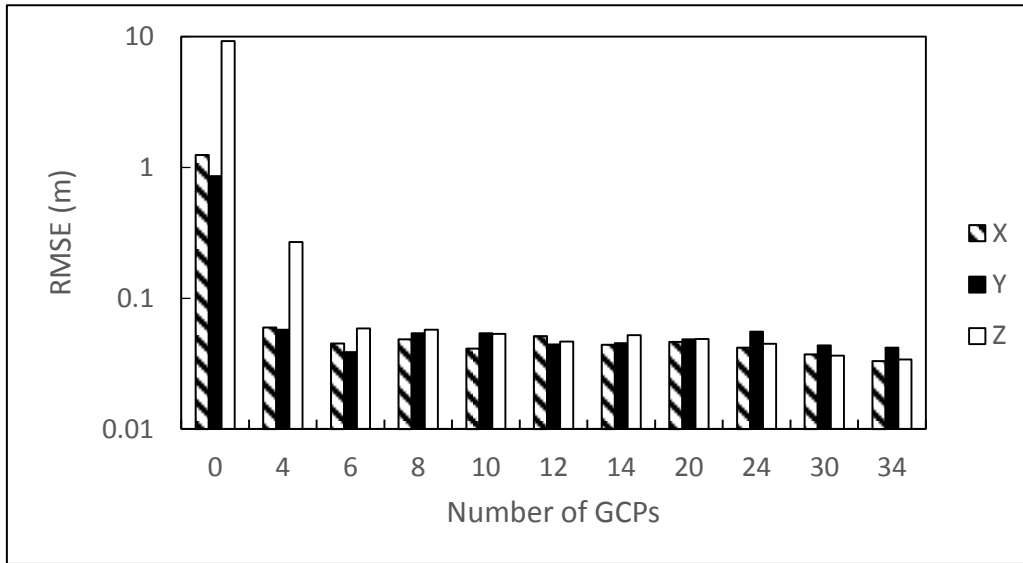
Figure 11: Number of GCPs and X, Y, Z RMSE. The z-coordinates' error decreased the most with increasing GCP amounts. Y-axis has a base-10 logarithmic scale.

4.4 Drone Type

The ebee RTK fixed-wing drone produced a model with a mean RMSE of 0.090-m, while the Phantom 3 Quadcopter produced a model with a mean RMSE of 0.040-m. Both of these flights were done at 80-m altitude, with 70% along-track and 75% across-track overlap. For the fixed-wing flight, most of the error came from the Y and Z coordinates, which produced RMSEs of 0.100-m and 0.090-m, respectively, with the X-coordinates producing a RMSE of only 0.042-m (see Figure 14). For the quadcopter, the X, Y, and Z RMSEs were 0.038-m, 0.045-m, and 0.038-m, respectively. From the single-factor ANOVA, a statistically significant difference was found between the XYZ absolute error of the fixed-wing flight and the quadcopter flight.
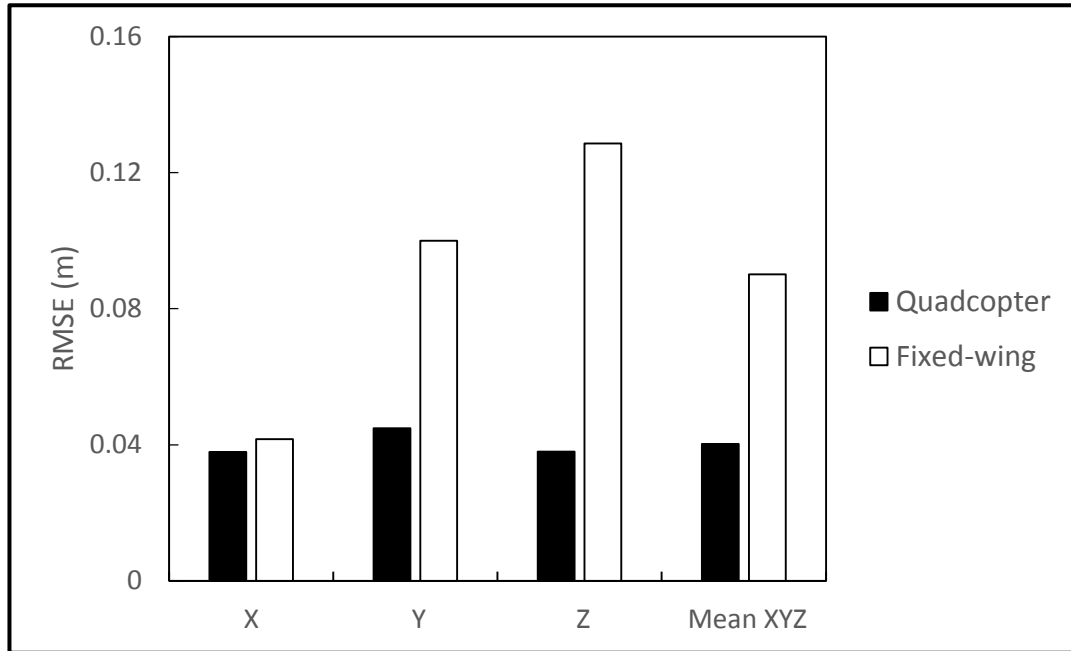
Figure 14: Drone model and RMSE. Fixed-wing drone has large elevation error (>10-cm).

4.5 Processing Software

For the 80-m, 70% along-track and 75% across-track overlap flight, Pix4D Desktop constructed a model with a mean RMSE of 0.040-m, while Agisoft PhotoScan constructed a model with a mean RMSE of 0.0296-m. The Agisoft models produced X, Y, and Z RMSEs of 0.026-m, 0.033-m, and 0.030-m, respectively, while the Pix4D desktop models produced X, Y, and Z RMSEs of 0.038-m, 0.045-m, and 0.038-m, respectively (see Figure 15). From the single-factor ANOVA, a statistically significant difference was found between the XYZ absolute error of the Pix4D Desktop model and the Agisoft PhotoScan model.
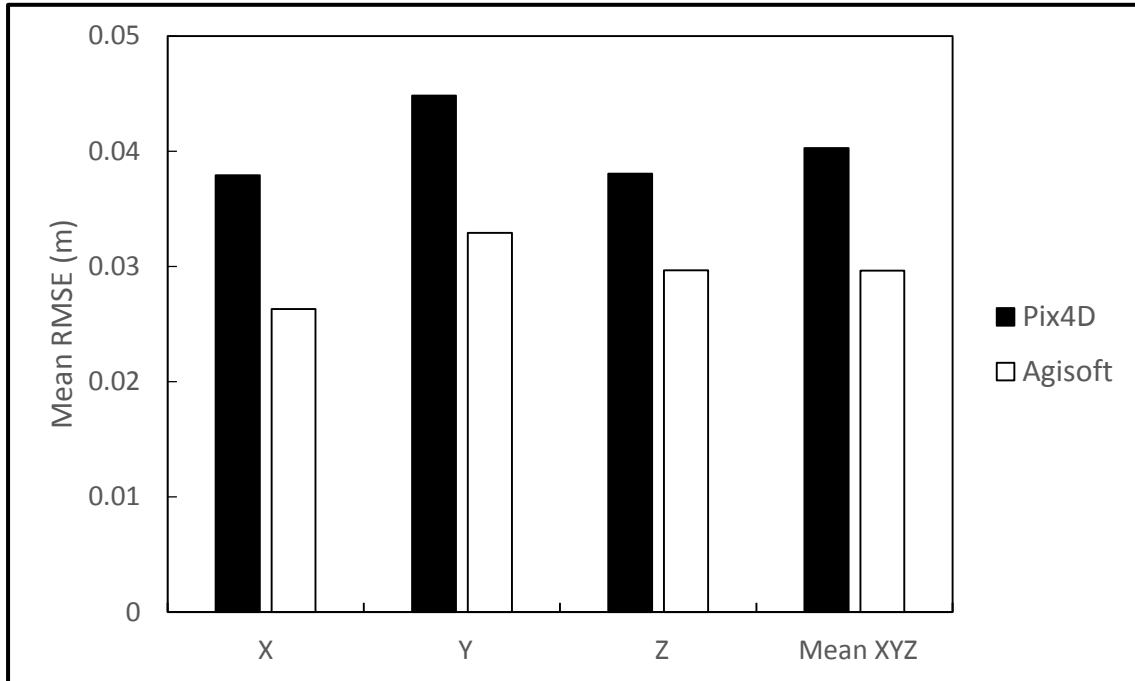
Figure 15: SfM software and RMSE. Agisoft models produce lower error in X, Y, and Z directions.

4.6 Raster and Point Cloud Comparisons

After conducting the raster and point cloud comparisons, distinct model differences were found between the 0 GCP and 6 GCP comparison; between the 4 GCP and 6 GCP comparison; and between the quadcopter and fixed-wing comparison (see Figures 16 and 17). The 0 GCP and 6 GCP comparison revealed similarity between horizontal coordinates, but a strong difference between elevation coordinates (16A, 16B, 17A, 17B, 17C). This difference in elevation shows strong fishbowl distortion in the 0 GCP model (elevated center and declined edges). The 4 GCP and 6 GCP comparison showed more similarity in X, Y, and Z coordinates, but there still remained some fishbowl distortion in the 4 GCP dataset,

28

giving this dataset a slightly convex shape (17D, 17E). For the quadcopter and fixed-wing comparison, absolute differences were mostly between 0.05-m and 1-m (17F, 17G, 17H). The point cloud comparisons, overall, showed more similarity between compared datasets relative to the raster comparisons.

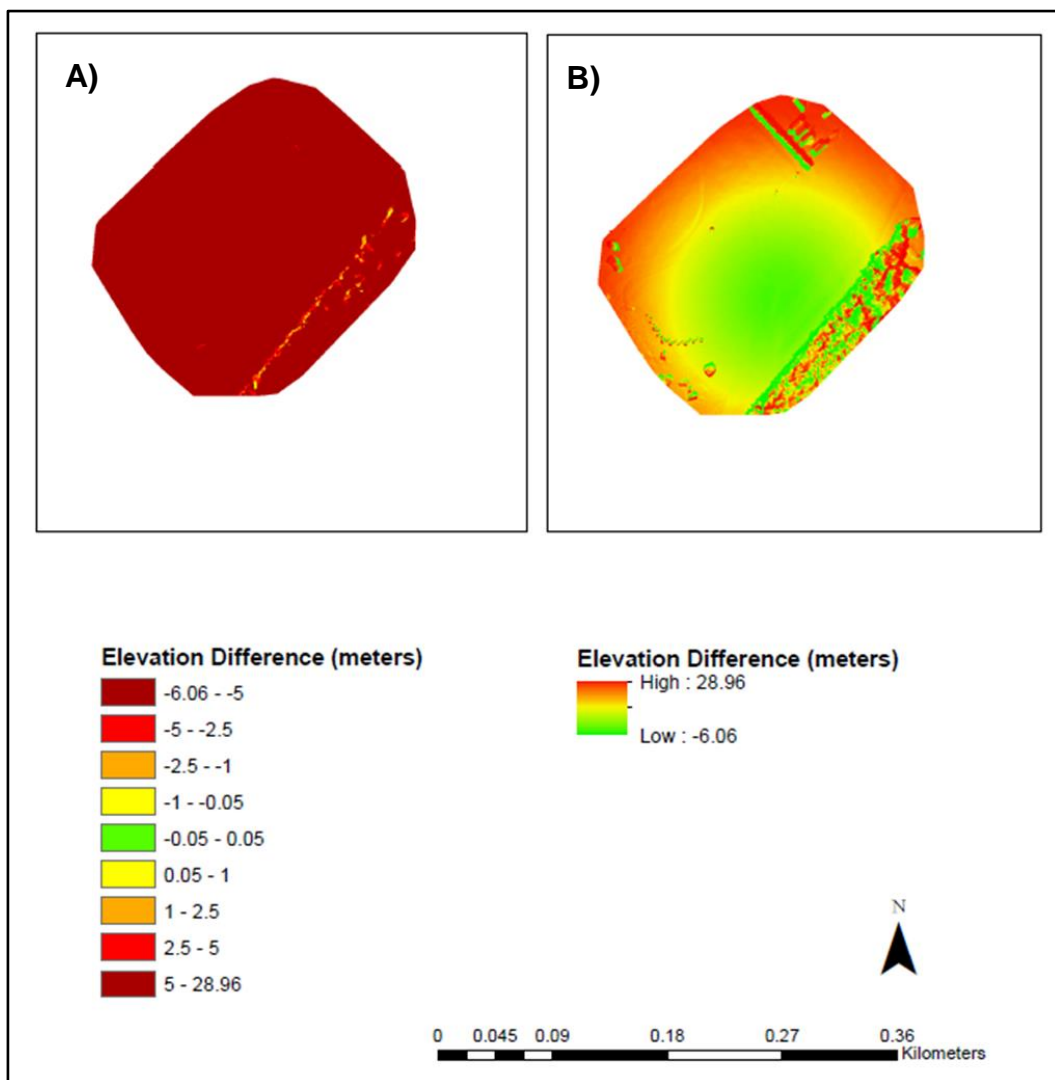Table 4 gives a comprehensive description of this study's mean RMSE results for each processed dataset.

Figure 16: Raster comparisons between 0 and 6 GCP datasets. A) Absolute difference scale. B) Stretched relative difference scale. The 0 GCP model had strong differences in elevation when compared to the 6 GCP model.
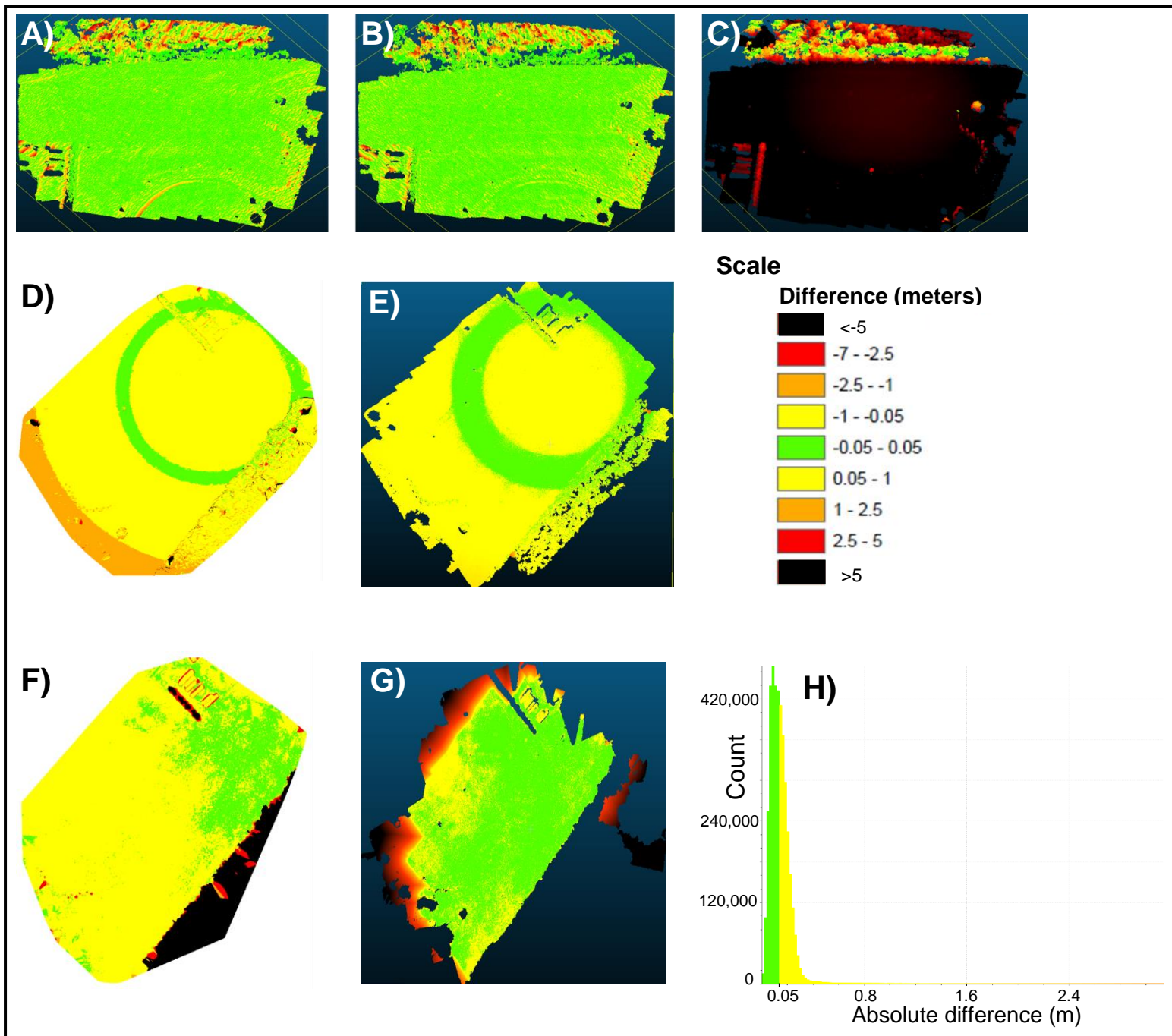
Figure 17: CloudCompare and ArcMap Results. A) Point cloud X-differences between 0 and 6 GCPs. B) Point cloud Y-differences between 0 and 6 GCP point clouds. C) Point cloud Z-differences between 0 and 6 GCP point clouds. D) Raster differences between 4 and 4 GCPs. E) Point cloud absolute differences between 4 and 6 GCPs. F) Raster differences between quadcopter and fixed-wing. G) Point cloud absolute differences between quadcopter and fixed-wing. H) Histogram of point cloud absolute differences between quadcopter and fixed-wing. All models have the same scale.

Table 4: Comprehensive mean RMSE results from this study.

Processing Software	Drone Type	Altitude (m)	Overlap % (Along/Across)	# of GCPs	Mean RMSE (m)
Pix4D Desktop	Quadcopter	80-m	80/80	0	3.778
Pix4D Desktop	Quadcopter	80-m	80/80	4	Even Spacing: 0.129 Random Spacing: 0.144
Pix4D Desktop	Quadcopter	80-m	80/80	6	Even Spacing: 0.047 Random Spacing: 0.049
Pix4D Desktop	Quadcopter	80-m	80/80	8	Even Spacing: 0.053 Random Spacing: 0.045
Pix4D Desktop	Quadcopter	80-m	80/80	10	Even Spacing: 0.050 Random Spacing: 0.049
Pix4D Desktop	Quadcopter	80-m	80/80	12	Even Spacing: 0.047 Random Spacing: 0.044
Pix4D Desktop	Quadcopter	80-m	80/80	14	Even Spacing: 0.047 Random Spacing: 0.047
Pix4D Desktop	Quadcopter	80-m	80/80	20	Even Spacing: 0.048 Random Spacing: 0.043
Pix4D Desktop	Quadcopter	80-m	80/80	24	Even Spacing: 0.047 Random Spacing: 0.043
Pix4D Desktop	Quadcopter	80-m	80/80	30	Even Spacing: 0.039 Random Spacing: 0.039
Pix4D Desktop	Quadcopter	80-m	80/80	34	0.036
Pix4D Desktop	Quadcopter	60-m	70/75	34	0.033
Pix4D Desktop	Quadcopter	120-m	70/75	34	0.043
Pix4D Desktop	Quadcopter	80-m	75/80	34	0.039
Pix4D Desktop	Fixed-wing	80-m	70/75	0	0.090
Agisoft PhotoScan	Quadcopter	80-m	70/75	34	0.030

5. Discussion

5.1 Optimal Altitude

Significant error variations occurred with varying altitudes. The 60-m flight produced the lowest error of any dataset processed in this study, with a mean RMSE of 0.033-m. However, the 120-m flight only brought up the mean RMSE error to 0.043-m. To minimize error and maximize efficiency, 80-m proves to be the best altitude to run surveys at, with a mean RMSE of 0.040-m. Performing a 60-m flight exponentially increases flight time relative to 80-m, especially when conducted over larger areas, and while it does decrease model error significantly, this difference is less than a centimeter. It would be inefficient to spend more time and battery life to bring model error down by only a few millimeters, particularly when the error is already near four centimeters. In studies that aim to have the highest precision data, lowering the altitude is the best method of decreasing the error in their models. However, these studies will be limited in the area they can cover, in addition to requiring more time for data collection and processing.

5.2 Optimal Photography Overlap Percentages

Using three separate 80-m altitude flights with varied overlap amounts, no significant difference was found in model error with respect to changing the amount of photography overlap. At 70% along-track overlap and 75% across-track overlap, the mean RMSE was 0.040-m, and only decreased to 0.036-m at 80% along-track and 80% across-track overlap.

Since increasing the amount of photography overlap will increase the flight time and make larger area flights a burden on battery life, it is inefficient to conduct UAV surveys at overlap amounts greater than 70% along-track and 75% across-track. This is especially true due to the ANOVA results. However, in a study done on densely vegetated areas, where precision in plant identification is needed, a higher overlap amount could be necessary (Zarco *et al.* 2014). As for studies tracking the movement, deposition, and erosion of sediment, 70% along-track and 75% across-track are sufficient overlap amounts.

5.3 Optimal GCP Amount and Spacing Scheme

For our 1.2-hectare study area, we determined that the optimum GCP ratio to survey area is six, or 0.20 hectares per GCP. Zero GCPs produced models with large elevation errors (>9-m), as well as horizontal errors greater than 1-m, giving the zero GCP model a distinct fishbowl distortion. Four GCPs decreased this error significantly, and six GCPs decreased the error significantly once again. However, there still remained fishbowl distortion in the 4 GCP model. Once more than six GCPs were added in data-processing, the error decrease became insignificant compared to the effort needed to place and measure, making the addition of more GCPs excessive and inefficient. As for the two spacing schemes tested, the difference in error produced by each spacing scheme was not significant, meaning that even or random spacing schemes can be used for the GCP placement. As long as there is uniform coverage throughout the study area, the GCPs do not need to be placed in precise, equally spaced increments throughout the site.

5.5 Type of GCP

Several types of GCPs were tested in this study by varying the size, color, and material. From a qualitative approach, spray paint was the easiest method to use, in contrast to laying down black and white tarps, and that each spray paint color used (yellow, blue, red, orange, white) all showed up to the user's eye in the photography. Each SfM software was able to identify each of the different GCP types as well. It is suggested that eco-friendly paint is used for GCP placement, to eliminate any detrimental environmental effects of a UAV survey.

5.6 Drone Type

The fixed-wing drone was shown to produce a model with a significantly higher error when compared to the quadcopter. However, the fixed-wing data was processed without the implementation of GCPs, relying on the drone's built-in RTK GPS system for scaling and georeferencing, while the quadcopter data was processed with 34 GCPs. This study suggests that when conducting a survey with an RTK-equipped fixed-wing drone, it is still necessary to include GCPs to obtain model errors below 0.05-m.

5.7 Processing Software

Since Agisoft and Pix4D produced significantly different errors, it is advised that future studies use multiple SfM software, to compare results and to ensure that results lead to

similar conclusions. In this particular study, the Agisoft models were shown to have less error than the Pix4D models, by approximately 1-cm in terms of mean RMSE. It would be highly beneficial to use data from future studies to compare Agisoft and Pix4D in terms of model error, in an effort to more conclusively decide which software produces lower RMSE over a variety of terrain.

5.8 Best Error Metric

While past studies have relied on the elevation RMSE extensively to quantify the error in 3D models, this study recommends the use of the mean RMSE for communicating a more-accurate error metric, as it encompasses all three coordinate directions into model error. The RMSE is more sensitive to outliers when compared to the MAE, causing it to penalize larger errors, thereby producing a larger error metric. In addition, when presenting the mean RMSE for a model, it is recommended that each coordinate's RMSE is presented as well to note any differences in error between the three separate coordinate directions.

6. Conclusions

This study provides insight for future implementation of the UAV/SfM methodology by providing RMSEs of models produced from various flight acquisition and post-processing parameters. The flight parameter tables can be referenced in future studies and provide guidance for optimizing UAV surveys. From the results of this study, it is suggested that the

following flight acquisition and post-processing parameters are used for efficient surveys and low-error models:

- 80-m flight altitude

- 70% along-track and 75% across-track photography overlap

- Six GCPs per hectare

- Addition of several GCPs in processing of eBee RTK fixed-wing drone data

- Even or random GCP spacing scheme, but with uniform coverage throughout study area

- Process data in more than one SfM software to compare results

- Present error with RMSE, for X, Y, and Z coordinates.

With more advancements in drone models, flight-planning software, data-processing software, and the automation of large portions of data analysis, the acquisition of high-accuracy and high precision data will become readily available to coastal scientists and other disciplines as well. These advancements will fuel future investigations, acting as powerful tools for answering difficult scientific questions.

Acknowledgements

project and the myriad of research experiences I gained throughout this spectacular summer.

Last, a special thanks to the Augustana geology and mathematics faculty (Dr. Michael Wolf,

Dr. Jeffery Strasser, Ms. Susan Wolf, Dr. Thomas Bengtson, Dr. Jon Claus, and Dr. Stacey

Rodman) for providing me with the support, tools, and knowledge to complete this senior

thesis.

References

Carrivick, J., Smith, M., and Quincey, D., 2012, Structure from Motion in the Geosciences: Hoboken, Wiley-Blackwell.

Casella, E., Rovere, A., Pedroncini, A., Stark, C., Casella, M., Ferrari, M., and Firpo, M., 2016, Drones as tools for monitoring beach topography changes in the Ligurian Sea (NW Mediterranean): Geo-Marine Letters, v. 36, p. 151-163, doi: 10.1007/s00367-016-0435-9.

Citton, P., Nicosia, U., Nicolosi, I., Carluccio, R., and Romano, M., 2015, Elongated theropod tracks from the Cretaceous Apenninic Carbonate Platform of southern Latium (central Italy: Palaeontologia Electronica.

Derrien, A., Villeneuve, N., Peltier, A., and Beauducel, F., 2015, Retrieving 65 years of volcano summit deformation from multitemporal structure from motion: The case of Piton de la Fournaise (La Réunion Island): Geophysical Research Letters, v. 42, p. 6959-6966, doi: 10.1002/2015GL064820.

Dietrich, J.T., 2017, Bathymetric Structure-from-Motion: extracting shallow stream bathymetry from multi-view stereo photogrammetry: Earth Surface Processes and Landforms, v. 42, p. 355-364, doi: 10.1002/esp.4060.

Dohner, S.M., Trembanis, A.C., and Miller, D.C., 2016, A tale of three storms: Morphologic response of Broadkill Beach, Delaware, following Superstorm Sandy, Huricane Joaquin, and Winter Storm Jonas: Shore and Beach, v. 84, p. 3-9.

Esposito, G., Mastrorocco, G., Salvini, R., Oliveti, M., and Starita, P., 2017, Application of UAV photogrammetry for the multi-temporal estimation of surface extent and volumetric excavation in the Sa Pigada Bianca open-pit mine, Sardinia, Italy: Environmental Earth Sciences, v. 76, p. 1-16, doi: 10.1007/s12665-017-6409-z.

Gomez, C., Hayakawa, Y., and Obanawa, H., 2015, A study of Japanese landscapes using structure from motion derived DSMs and DEMs based on historical aerial photographs: New opportunities for vegetation monitoring and diachronic geomorphology: Geomorphology, v. 242, p. 11-20, doi: 10.1016/j.geomorph.2015.02.021.

Harwin, S., and Lucieer, A., 2012, Assessing the Accuracy of Georeferenced Point Clouds Produced via Multi-View Stereopsis from Unmanned Aerial Vehicle (UAV) Imagery: Remote Sensing, v. 4, p. 1573-1599, doi: 10.3390/rs4061573.

Holman, R.A., Brodie, K.L., and Spore, N.J., 2017, Surf Zone Characterization Using a Small Quadcopter: Technical Issues and Procedures: IEEE Transactions on Geoscience and Remote Sensing, v. 55, p. 2017-2027, doi: 10.1109/TGRS.2016.2635120.

Holman, R., Plant, N., and Holland, T., 2013, cBathy: A robust algorithm for estimating nearshore bathymetry: Journal of Geophysical Research: Oceans, v. 118, p. 2595-2609, doi: 10.1002/jgrc.20199.

Hugenholtz, C.H., Whitehead, K., Brown, O.W., Barchyn, T.E., Moorman, B.J., LeClair, A., Riddell, K., and Hamilton, T., 2013, Geomorphological mapping with a small unmanned aircraft system (sUAS): Feature detection and accuracy assessment of a photogrammetrically-derived digital terrain model: Geomorphology, v. 194, p. 16-24, doi: 10.1016/j.geomorph.2013.03.023.

Hyatt, J.A., Using scanning and photogrammetry to develop objective geometric measures and educational resources for a *Eubrontes* tracksite, Dinosaur state Park, CT: Abstract 37-03 presented at 2017 Geological Society of America Joint Meeting Northeastern/North-Central Sections, Pittsburgh, Pennsylvania, 19-31 March.

James, M.R., and Robson, S., 2014, Mitigating systematic error in topographic models derived from UAV and ground- based image networks: Earth Surface Processes and Landforms, v. 39, p. 1413-1420, doi: 10.1002/esp.3609.

Jaud, M., Passot, S., Le Bivic, R., Delacourt, C., Grandjean, P., and Le Dantec, N., 2016, Assessing the Accuracy of High Resolution Digital Surface Models Computed by PhotoScan® and MicMac® in Sub-Optimal Survey Conditions: Remote Sensing, v. 8, p. 465, doi: 10.3390/rs8060465.

Nathalie Long, Bastien Millescamps, Benoît Guillot, Frederic Pouget, and Xavier Bertin, 2016, Monitoring the Topography of a Dynamic Tidal Inlet Using UAV Imagery: Remote Sensing, v. 8, p. 387, doi: 10.3390/rs8050387.

Nex, F., and Remondino, F., 2014, UAV for 3D mapping applications: a review: Applied Geomatics, v. 6, p. 1-15, doi: 10.1007/s12518-013-0120-x.

Scarelli, F.M., Sistilli, F., Fabbri, S., Cantelli, L., Barboza, E.G., and Gabbianelli, G., 2017, Seasonal dune and beach monitoring using photogrammetry from UAV surveys to apply in the ICZM on the Ravenna coast (Emilia-Romagna, Italy): Remote Sensing Applications: Society and Environment, v. 7, p. 27-39.

Tamminga, A.D., Eaton, B.C., and Hugenholtz, C.H., 2015, UAS-based remote sensing of fluvial change following an extreme flood event: Earth Surface Processes and Landforms, v. 40, p. 1464-1476, doi: 10.1002/esp.3728.

Tonkin, T., and Midgley, N., 2016, Ground-Control Networks for Image Based Surface Reconstruction: An Investigation of Optimum Survey Designs Using UAV Derived Imagery and Structure-from-Motion Photogrammetry: Remote Sensing, v. 8, p. 786, doi: 10.3390/rs8090786.

Turner, I.L., Harley, M.D., and Drummond, C.D., 2016, UAVs for coastal surveying: Coastal Engineering, v. 114, p. 19-24, doi: 10.1016/j.coastaleng.2016.03.011.

Westoby, M.J., Brasington, J., Glasser, N.F., Hambrey, M.J., and Reynolds, J.M., 2012, 'Structure-from-Motion' photogrammetry: A low-cost, effective tool for geoscience applications: Geomorphology, v. 179, p. 300-314, doi: 10.1016/j.geomorph.2012.08.021.

Zarco-Tejada, P.J., Diaz-Varela, R., Angileri, V., and Loudjani, P., 2014, Tree height quantification using very high resolution imagery acquired from an unmanned aerial vehicle (UAV) and automatic 3D photo-reconstruction methods: European Journal of Agronomy, v. 55, p. 89-99, doi: 10.1016/j.eja.2014.01.004.

Appendix A: Past Studies on UAV/SfM Model Accuracy

Reference/Topic	Topic	UAV/Altitude	# of GCPs	Hectares Per GCP	SfM Software	Comparison Data	Error (m)
Hugenholtz *et al.* 2013	Aeolian geomorphology	Hawkeye RQ-84Z Areohawk fixed-wing 200-m	28	6.86	Trimble Inpho	RTK GPS	RMSE (z) = 0.29
Tamminga *et al.* 2015	Fluvial geomorphology	Aeryon Scout quadcopter 100-m	45	0.18	Pix4D	RTK GPS	RMSE (z) = 0.095
Tonkin and Midgley 2016	Glacial environmental photogrammetry	DJI S800 hexacopter 100-m	3, 4, 5, 7, 8, 9, 10, 15, 20, 25, 30, 40, 50, 60, 80, 101	4.83, 3.63, 2.90, 2.07, 1.81, 1.61, 1.45, 0.97, 0.73, 0.28, 0.48, 0.36, 0.29, 0.24, 0.18 0.14	Agisoft PhotoScan	dGPS	RMSE (z) = 0.156, 0.064, 0.060, 0.062, 0.073, 0.063, 0.075, 0.076, 0.073, 0.073, 0.067, 0.066, 0.060, 0.064, 0.061, 0.059
Jaud *et al.* 2016	UAV/SfM methodology	DroneSys DS6 hexacopter 100-m	12	0.58	Agisoft PhotoScan	RTK DGPS	RMSE (xy) = 0.045 RMSE (z) = 0.039
					MicMac		RMSE (xy) = 0.035 RMSE (z) = 0.032
					Agisoft PhotoScan	TLS	Mean difference = 0.05
					MicMac		Mean difference = 0.22
Long *et al.* 2016	Coastal geomorphology	SenseFly eBee fixed-wing 150-m	24	16.67	Agisoft PhotoScan	GNSS	RMSE (z) = 0.17
Casella *et al.* 2016	Coastal geomorphology	RPAS Mikrokopter Okto XL 80-m	9	0.11	Agisoft PhotoScan	DGPS	RMSE (z) = 0.16
Dohner *et al.* 2016	Coastal geomorphology	DJI Phantom 3 Advanced 80-m	0	N/A	Agisoft PhotoScan	RTK GPS	Mean (xy and z) = 0.02 to 0.05
Turner *et al.* 2016	Coastal geomorphology	SenseFly eBee-RTK 100-m	0 (UAV equipped with RTK GPS)	N/A	Pix4D	RTK GPS	Mean (z) = 0.026
Scarelli *et al.* 2017	Coastal geomorphology	SAL Engineering VTOL hexacopter 60-m	65, 108	1.54, 0.93	Agisoft PhotoScan	RTK GPS	RMSE (z) = 0.0605, 0.0522